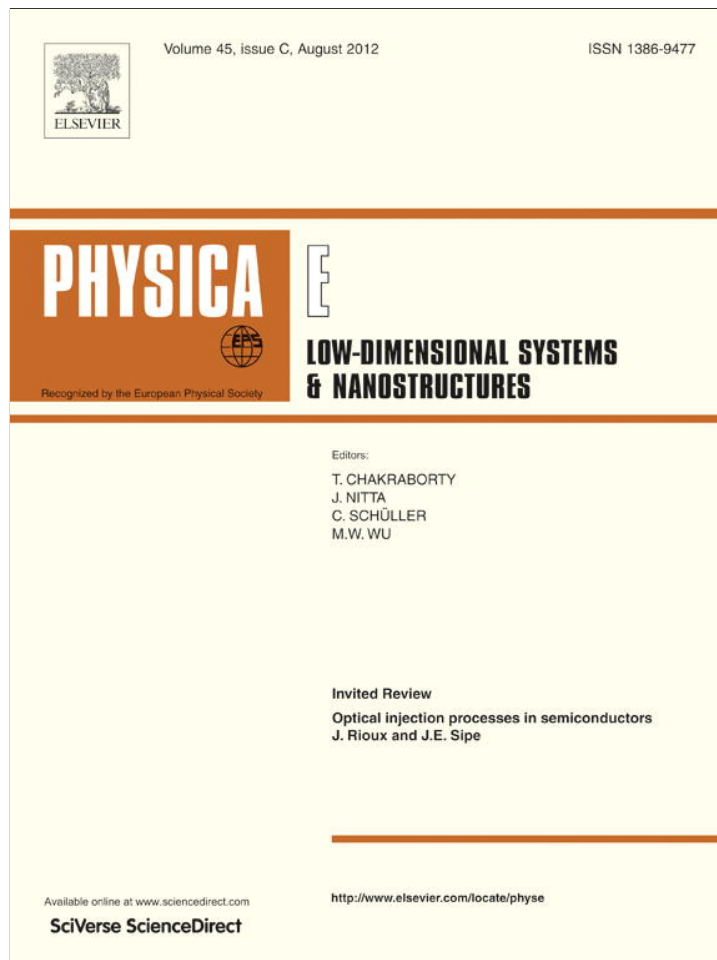


Provided for non-commercial research and education use.
Not for reproduction, distribution or commercial use.

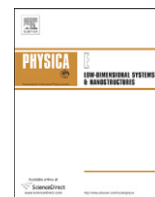


This article appeared in a journal published by Elsevier. The attached copy is furnished to the author for internal non-commercial research and education use, including for instruction at the authors institution and sharing with colleagues.

Other uses, including reproduction and distribution, or selling or licensing copies, or posting to personal, institutional or third party websites are prohibited.

In most cases authors are permitted to post their version of the article (e.g. in Word or Tex form) to their personal website or institutional repository. Authors requiring further information regarding Elsevier's archiving and manuscript policies are encouraged to visit:

<http://www.elsevier.com/copyright>



Classical magnetoresistance of a ballistic electron gas constrained to non-planar topographies in a lattice of antidots under tilted magnetic field

N.M. Sotomayor^{a,*}, L.A. Cabral^a, L.Y.A. Davila^a, G.M. Gusev^b

^a Universidade Federal do Tocantins, Campus Universitário de Araguaína, TO, Brazil

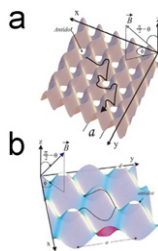
^b Instituto de Física da Universidade de São Paulo, Caixa Postal 66318, CEP 05315-970, São Paulo, Brazil

HIGHLIGHTS

- ▶ A classical ballistic two-dimensional electron gas subjected to constraints is modeled.
- ▶ Geometrical constraints coupled the degrees of freedom and introduced additional drift and disorder.
- ▶ Low field magnetoresistance in antidote lattice evolves to negative behavior when disorder increases.
- ▶ Constraints introduce chaos in electron transport.

GRAPHICAL ABSTRACT

Scheme of two different surfaces for the numerical modeling of the classical dynamics of a two-dimensional electron gas in antidot lattices constrained to non-planar topographies, in uniform magnetic field, used in this work. (a) Topography modeled by the surface $f_1(x,y)$ “wrinkled strips”. (b) Topography modeled by the surface $f_2(x,y)$ “eggbox”. The black solid lines represent electron trajectories and the white circles the forbidden regions occupied by the antidots.



ARTICLE INFO

Article history:

Received 24 February 2012

Received in revised form

15 July 2012

Accepted 17 July 2012

Available online 26 July 2012

ABSTRACT

The classical magnetoresistance of a two-dimensional electron gas constrained to non-planar topographies, in antidot lattices, and under the influence of tilted magnetic field in arbitrary direction is numerically studied.

© 2012 Elsevier B.V. All rights reserved.

1. Introduction

In the last years, the theoretical and experimental study of the transport properties of a ballistic two-dimensional electron gas (2DEG), in semiconductor crystals, under spatially fluctuating magnetic fields, has attracted lot of attention in condensed-matter physics [1–6]. Experimentally, samples containing a 2DEG that is influenced by magnetic fields that vary with position were obtained by different methods such as the deposition of several or only one nanometric-width ferromagnetic stripes on top of semiconductor heterojunctions [7,8], by growing a remotely

doped GaAs/AlGaAs heterostructure over a cleaned wafer previously pre-patterned with etched facets [9], by deposition of arrays of superconducting stripes on the surface of a heterostructure [10], by regrowth of a 2DEG heterostructure over dimpled surfaces [11], by attaching NdFeB magnets on top of high mobility GaAs/AlGaAs heterostructures [5], and more recently, by a regrowth process of a GaAs/AlGaAs high electron mobility transistor (HEMT) structures over antidot lattices, previously pre-patterned on cleaned semi-insulating GaAs substrates [12–14].

These experimental realizations made it possible to observe and analyze interesting magnetotransport phenomena between the classical and quantizing magnetic field regimes. At weak magnetic field values, when the classical cyclotron diameter R_c is equal to the periodicity of the magnetic field fluctuations, commensurability oscillations were observed in magnetoresistance

* Corresponding author. Tel.: +55 63 34153379.

E-mail address: nmsotomayor@pq.cnpq.br (N.M. Sotomayor).

ρ_{xx} [8]. In semiconductor systems where a 2DEG is constrained to quasi-periodic or random surfaces and subject to a uniform magnetic field, in arbitrary direction, corrugations produce an effective sign alternating magnetic field where fluctuation may have or not a zero average $\langle B \rangle = 0$. These systems display strong negative or positive deviations of magnetoresistance from a constant behavior predicted by the Boltzmann–Drude approach [14,15]. A recent study in GaAs/AlGaAs samples, that constrain electrons to random surface topographies, showed an anomalous large linear decrease of magnetoresistance (LNMR) that reached up to 20% of the zero field resistivity. This anomalous LNMR was explained through non-Markovian effects showing the importance of considering memory related effects in magnetotransport of a 2DEG at the classical level [14]. Negative and positive deviations from a constant behavior of magnetoresistance were also attributed to manifestations of weak localization, and the interplay of strong scatterers and a smooth random potential.

Theoretical analysis have pointed out the existence of extended states in a two-dimensional electron gas in a spatially random field with zero average [1], also a relation between a high- T_c superconductivity and the problem of random field was found. More recently a close relation between the motion of electrons in a random magnetic field around $B=0$ and composite fermions near even denominator in the fractional quantum Hall states was discovered. The present work is focused on the classical electron dynamics of a non-interacting 2DEG constrained to non-planar periodic topographies, in a tunable lattice of antidots, and subjected to an external magnetic field oriented in arbitrary direction in relation to the sample surface. The aim is to obtain a classical approximation and description of the anomalous low field magnetoresistance observed in 2DEG samples with high degree of disordered and fluctuating magnetic field [14].

This paper is organized as follows, in Section 2 we describe the theoretical model for the dynamics of the 2DEG in the presence of uniform magnetic field, antidot lattice, and geometrical constraints showing explicit expressions for the motion equations, still in this section, the numerical integration of the motion equations and the calculation of the longitudinal and transversal resistivities are detailed. In Section 3 we present the numerical results for the longitudinal and Hall resistances for the 2DEG, with and without antidot lattices, in perpendicular and tilted magnetic field for two types of geometrical constraints. Simultaneously, the evolution of the resistivities is analyzed by means of the perturbation of phase space through Poincaré surfaces of the section.

2. Theoretical model

A classical description of the low field magnetoresistance in a 2DEG in GaAs/AlGaAs corrugated samples, with a high degree of disorder, can be obtained departing from the dynamics of two-dimensional electrons constrained to move in periodic non-planar topographies in the presence of antidot lattices and uniform perpendicular magnetic field oriented in arbitrary direction in relation to the sample surface. Fig. 1(a) and (b) illustrates schematically different numerical electron trajectories constrained to two different non-planar topographies modeled by geometrical functions, the lattice of antidots and the direction of the magnetic field vector.

In order to obtain this dynamics we depart from the single particle Lagrangian:

$$L = \frac{1}{2}m^*v^2 - e\vec{v} \cdot \vec{A} + \lambda\Phi - U_{ad}(x,y), \quad (1)$$

where m^* is the electron effective mass, v is the electron velocity, e is the electron charge, λ is a Lagrange multiplier and $\Phi = z - f_i(x,y)$, $i = 1,2$ is a geometrical constraint that models the

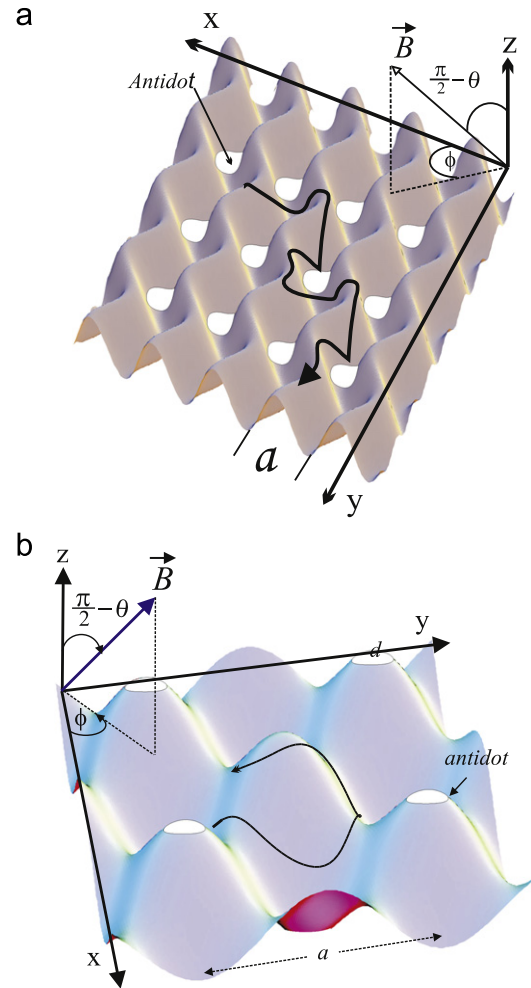


Fig. 1. Scheme of two different surfaces for the numerical modeling of the classical dynamics of a two-dimensional electron gas in antidot lattices constrained to non-planar topographies, in uniform magnetic field, used in this work. (a) Topography modeled by the surface $f_1(x,y)$ “wrinkled strips”. (b) Topography modeled by the surface $f_2(x,y)$ “eggbox”. The black solid lines represent electron trajectories and the white circles the forbidden regions occupied by the antidots.

topography of the 2DEG. For this work, two periodic surfaces named f_1 “wrinkled strips”, and f_2 “eggbox” were chosen, they are modeled by the following expressions:

$$f_1(x,y) = A \cos(K[x + D \cos(My)]), \quad (2)$$

$$f_2(x,y) = A \cos(Kx) \cos(Ky), \quad (3)$$

where A and D are parameters to tune the amplitude of corrugations and K and M accounts for the period of corrugations along x and y directions (for this work $K = M = 2\pi$). A uniform magnetic field B oriented in arbitrary direction, in relation to the surface of the sample, can be obtained from the potential vector \vec{A} given by

$$\vec{A} = \frac{B}{2}(-y \sin \theta + z \cos \theta \sin \phi, x \sin \theta - z \cos \theta \cos \phi, y \cos \theta \cos \phi - x \cos \theta \sin \phi), \quad (4)$$

where θ is the angle between the magnetic field vector and its projection to the x – y plane, and ϕ is the angle between this projection and the x -axis.

The electrostatic potential due to the antidot lattices is modeled by Eq. (5), the maximum amplitude can be tuned through the parameter U_0 . a is the period of the lattice and β

accounts for the steepness of the potential:

$$U_{ad}(x,y) = U_0 \left[\cos\left(\frac{\pi x}{a}\right) \cos\left(\frac{\pi y}{a}\right) \right]^\beta. \quad (5)$$

Introduction of the canonically conjugate momenta leads to the Hamilton formalism. The Hamilton–Dirac method for systems including second class constraints was used [16,17], according to this model, the extended Hamiltonian of the system is given by

$$H_e(\vec{p}, \vec{r}) = H_c - \Phi_a \mathbf{C}_{ab}^{-1}(\Phi_b, H_c), \quad (6)$$

where $\vec{r} = (x,y,z)$, $\vec{p} = (p_x, p_y, p_z)$ are the position and momentum vectors, respectively. The indexes a and b assume the values 1,2 and $H_c = 1/2m^*(\vec{p} + e\vec{A})^2 - \lambda\Phi + U_{ad}(x,y)$. $\Phi_1 = z - f_1(x,y) = 0$ and $\Phi_2 = (1/m^*)\vec{p} \cdot \vec{\nabla}\Phi_1 = 0$ are second class constraints with $\vec{P} = \vec{p} - e\vec{A}$. The matrix \mathbf{C}_{ab}^{-1} is the inverse matrix obtained out of the Poisson brackets:

$$\mathbf{C}_{ab} = \begin{bmatrix} \{\Phi_a, \Phi_a\} & \{\Phi_a, \Phi_b\} \\ \{\Phi_b, \Phi_a\} & \{\Phi_b, \Phi_b\} \end{bmatrix}. \quad (7)$$

We use dimensionless variables:

$$\tilde{H} = \frac{H}{E_F}, \quad \tilde{U}_{ad} = \frac{U_{ad}}{E_F}, \quad \tilde{B} = \frac{B}{B_0}, \quad (8)$$

where E_F is the Fermi energy.

$$\tilde{x} = \frac{x}{a}, \quad \tilde{y} = \frac{y}{a}, \quad \tilde{z} = \frac{z}{a}, \quad \tilde{t} = \frac{t}{\tau_0}. \quad (9)$$

As units to scale time and magnetic field we use

$$\tau_0 = \left(\frac{m^* a^2}{2E_F} \right)^{1/2}, \quad B_0 = \frac{2(2m^* E_F)^{1/2}}{ea}, \quad (10)$$

where τ_0 corresponds to the time that an electron delays in traveling a lattice distance a at the Fermi speed, and B_0 corresponds to a cyclotron radius of half the length of the period a of the artificial lattice. In terms of dimensionless units, and omitting tildes, the Hamiltonian can be written as

$$H_c = [p_x + B(z \cos \theta \sin \phi - y \sin \theta)]^2 + [p_y + B(x \sin \theta - z \cos \theta \cos \phi)]^2$$

$$+ [p_z + B(y \cos \theta \cos \phi - x \cos \theta \sin \phi)]^2 - \lambda\Phi + U_{ad}(x,y). \quad (11)$$

In the next, the Hamilton–Dirac algorithm for constrained systems is used. By verifying if the evolution generated by the Hamiltonian preserves the primary constraint $\Phi = 0$ yields a secondary constraint, from here on called $\Psi = \{\Phi, H_c\}$. In the next subsection, the calculations for each of the two specific constraint models, studied in this work, is detailed.

2.1. Obtention of the motion equations for the two geometrical constraints

2.1.1. f_1 topography

For the case of a topography of the type $f_1(x,y)$,

$$\Psi = 2AK \sin \gamma P_x - 2AKDM \sin(My) \sin \gamma P_y + 2P_z = 0, \quad (12)$$

where the next substitutions were used in order to show the equations in a compact way:

$$\begin{aligned} \gamma &= K(x + D \cos[My]), \\ P_x &= [p_x + B(z \cos \theta \sin \phi - y \sin \theta)], \\ P_y &= [p_y + B(x \sin \theta - z \cos \theta \cos \phi)], \\ P_z &= [p_z + B(y \cos \theta \cos \phi - x \cos \theta \sin \phi)]. \end{aligned} \quad (13)$$

By checking if the secondary constraint is preserved by time evolution $\{\Psi, H_c\} = 0$, we obtain an expression $\Psi(\vec{r}, \vec{p}, \lambda) = 0$, and use this expression to determine

$$\begin{aligned} \lambda &= \alpha \left(-2AK^2 \cos \gamma P_x^2 + 4AK^2 DM \sin(My) \cos \gamma P_x P_y \right. \\ &\quad + 4ABKDM \sin \theta \sin(My) \sin \gamma P_x \\ &\quad + 4B \cos \theta \sin \phi P_x + 4ABK \sin \theta \sin \gamma P_y \\ &\quad - 4ABK \cos \theta \sin \phi \sin \gamma P_z \\ &\quad + 2AKDM^2 \cos(My) \sin \gamma P_y^2 - 2A(KDM)^2 \sin^2(My) \cos \gamma P_y^2 \\ &\quad \left. - 4B \cos \theta \cos \phi P_y^2 - 4ABKDM \sin(My) \cos \theta \cos \phi \sin \gamma P_z \right. \\ &\quad \left. AK \sin \gamma \frac{\partial U_{ad}}{\partial x} - AKDM \sin(My) \sin \gamma \frac{\partial U_{ad}}{\partial y} \right), \end{aligned} \quad (14)$$

where

$$\alpha = \frac{1}{1 + (AK \sin \gamma)^2 + (AKDM \sin(My))^2 \sin^2 \gamma}. \quad (15)$$

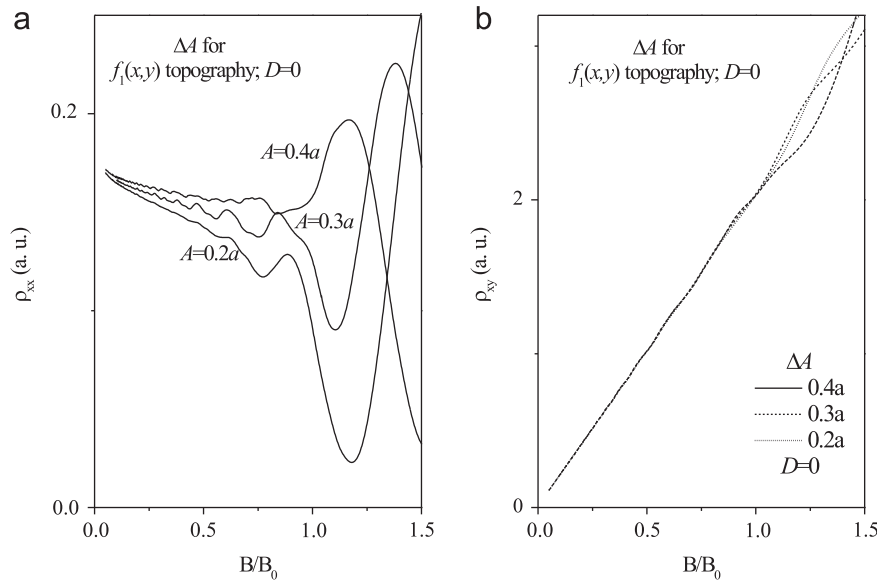


Fig. 2. Numerical (a) ρ_{xx} and (b) ρ_{xy} curves at low field for the 2DEG constrained to $f_1(x,y)$ topography. For these calculations the parameters $\theta = \pi/2$, $\phi = 0$, $U_0 = 0$, $D = 0$ were used. The amplitude of the corrugations A , in the x direction, was varied for the values $A = 0.2a$, $A = 0.3a$, and $A = 0.4a$. Commensurability oscillations at ρ_{xx} are present, their amplitude increase inversely to the cyclotron radius.

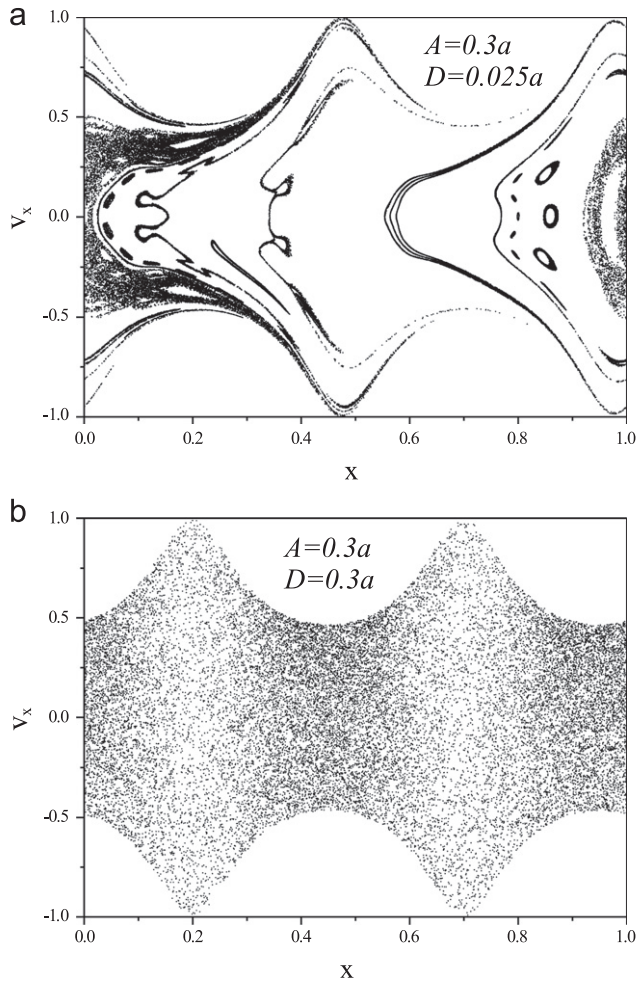


Fig. 3. Two Poincaré surfaces of section at $[y(\text{mod } 1) = 0]$ for the 2DEG constrained to $f_1(x,y)$ topography. For these calculations $\theta = \pi/2$, $\phi = 0$, and $U_0 = 0$ were used. In (a) there is small coupling between x – y degrees of freedom and most trajectories are periodic. In (b) there is strong modulation along x and y direction that produce a chaotic phase space.

By taking brackets with the Hamiltonian we obtain six motion equations:

$$\begin{aligned} \dot{x} &= 2P_x, \\ \dot{y} &= 2P_y, \\ \dot{z} &= 2P_z, \\ \dot{p}_x &= -2\frac{B}{B_0} \sin \theta P_y + 2\frac{B}{B_0} \cos \theta \sin \phi P_z + \lambda AK \sin(Kx) \cos(Ky) - \frac{\partial U_{ad}(x,y)}{\partial x}, \\ \dot{p}_y &= 2\frac{B}{B_0} \sin \theta P_x - 2\frac{B}{B_0} \cos \theta \cos \phi P_z + \lambda AK \cos(Kx) \sin(Ky) - \frac{\partial U_{ad}(x,y)}{\partial y}, \\ \dot{p}_z &= -2\frac{B}{B_0} \cos \theta \sin \phi P_x + 2\frac{B}{B_0} \cos \theta \cos \phi P_y + \lambda. \end{aligned} \quad (16)$$

2.1.2. f_2 topography

For the case of a topography of the type $f_2(x,y)$,

$$\Psi = 2AK \sin(Kx) \cos(Ky) P_x - 2AK \cos(Kx) \sin(Ky) P_y + 2P_z = 0, \quad (17)$$

where again substitutions given by Eqs. (13) were used.

Following the Hamilton–Dirac algorithm, we arrive to another expression for λ as

$$\begin{aligned} \lambda &= \alpha \left(-2AK^2 \cos(Kx) \cos(Ky) P_x^2 + 4AK^2 \sin(Kx) \sin(Ky) P_x P_y \right. \\ &\quad - 4ABK \sin \theta \cos(Kx) \sin(Ky) P_x + 4B \cos \theta \sin \phi P_x \\ &\quad + 4ABK \sin \theta \sin(Kx) \cos(Ky) P_y - 4BK \cos \theta \sin \phi \sin(Kx) \cos(Ky) P_z \\ &\quad - 2AK^2 \cos(Kx) \cos(Ky) P_y^2 - 4B \cos \theta \cos \phi P_y \\ &\quad + 4ABK \cos \theta \cos \phi \cos(Kx) \sin(Ky) P_z \\ &\quad \left. + AK \sin(Kx) \cos(Ky) \frac{\partial U_{ad}}{\partial x} + AK \cos(Kx) \sin(Ky) \frac{\partial U_{ad}}{\partial y} \right), \end{aligned} \quad (18)$$

where

$$\alpha = \frac{1}{A^2 K^2 [\sin(Kx)^2 \cos(Ky)^2 + \cos(Kx)^2 \sin(Ky)^2] + 1}. \quad (19)$$

In this case the motion equations are again given by Eq. (16) with λ and α given by Eqs. (18) and (19), respectively.

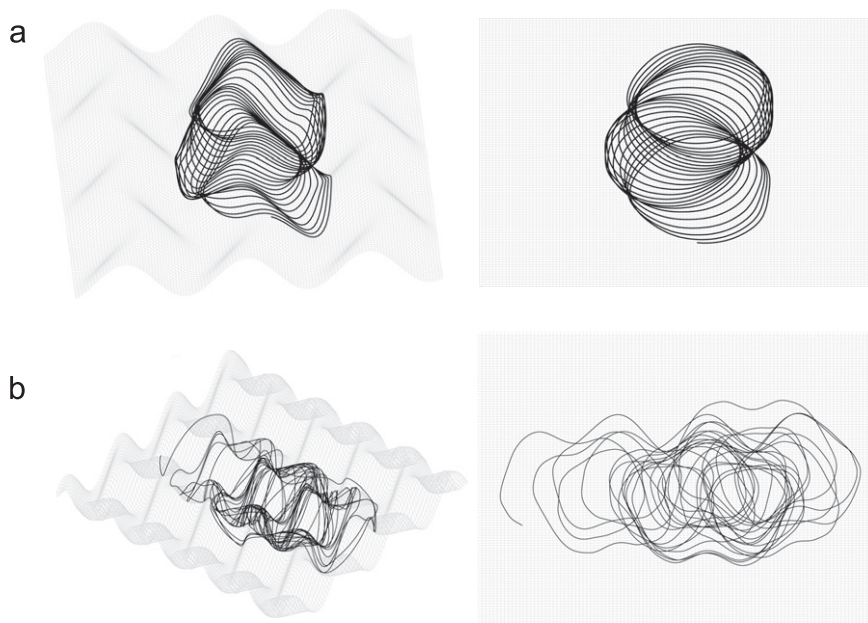


Fig. 4. Numerical trajectories for surface $f_1(x,y)$. (a) For low x – y coupling ($A=D=0.05a$), left side: lateral view, right side: top view. (b) For strong coupling ($A=D=0.3a$).

2.2. Model for the ohmic conductivity

We used a fifth and sixth order Runge–Kutta–Verner methods to numerically integrate these two system of differential equations and obtain the electron trajectories. The numerical integration of these equations of motion allows us to study the evolution of phase space Γ by means of Poincaré surfaces of the section. Also, the longitudinal and transversal resistivities were calculated by means of classical linear response theory [18], according to

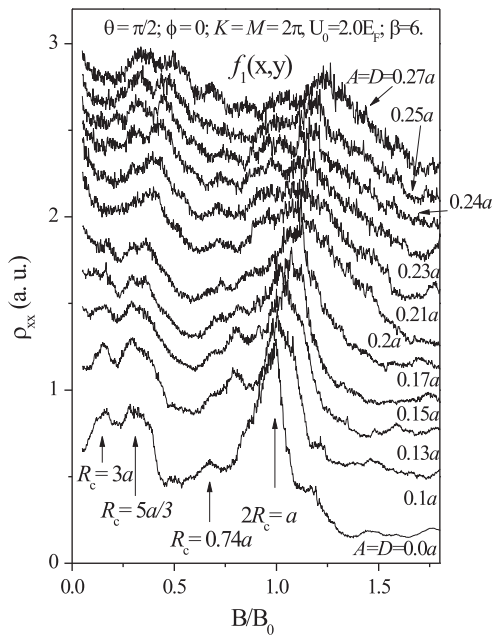


Fig. 5. Numerical magnetoresistance of a 2DEG constrained to a topography modeled by $f_1(x,y)$ in a lattice of antidots in perpendicular magnetic field. The amplitudes of the corrugations along x – y directions were varied from $A = D = 0$ to $A = D = 0.27a$, other parameters used are $U_0 = 2.0E_F$, $\beta = 6$, $\theta = \pi/2$ and $\phi = 0$. As A and D are increased commensurability peaks are destroyed and magnetoresistance turns negative.

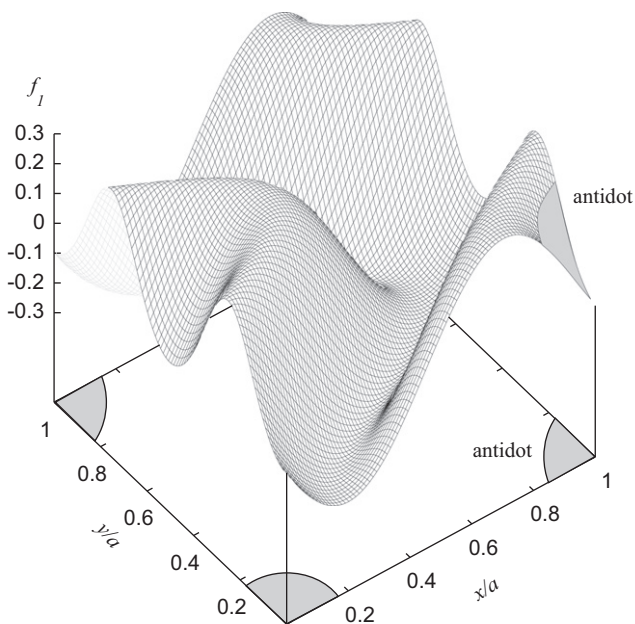


Fig. 6. Unit cell of period a for the antidot lattice. When the topography of the 2DEG is planar the cross section of the antidot at the Fermi energy is circular, when the topography is corrugated along the x and y directions the cross section of the antidot changes to elliptical.

this, the ohmic conductivity σ_{ij} is proportional to the diffusivity and is given by the expression:

$$\sigma_{ij} = \frac{N_s e^2}{E_F} \int_0^\infty \langle v_i(t)v_j(t=0) \rangle_\Gamma e^{-t/\tau} dt, \quad (20)$$

where N_s is the electron concentration, E_F is the Fermi energy, $\langle v_i(t)v_j(0) \rangle_\Gamma$ is the velocity–velocity correlation function double

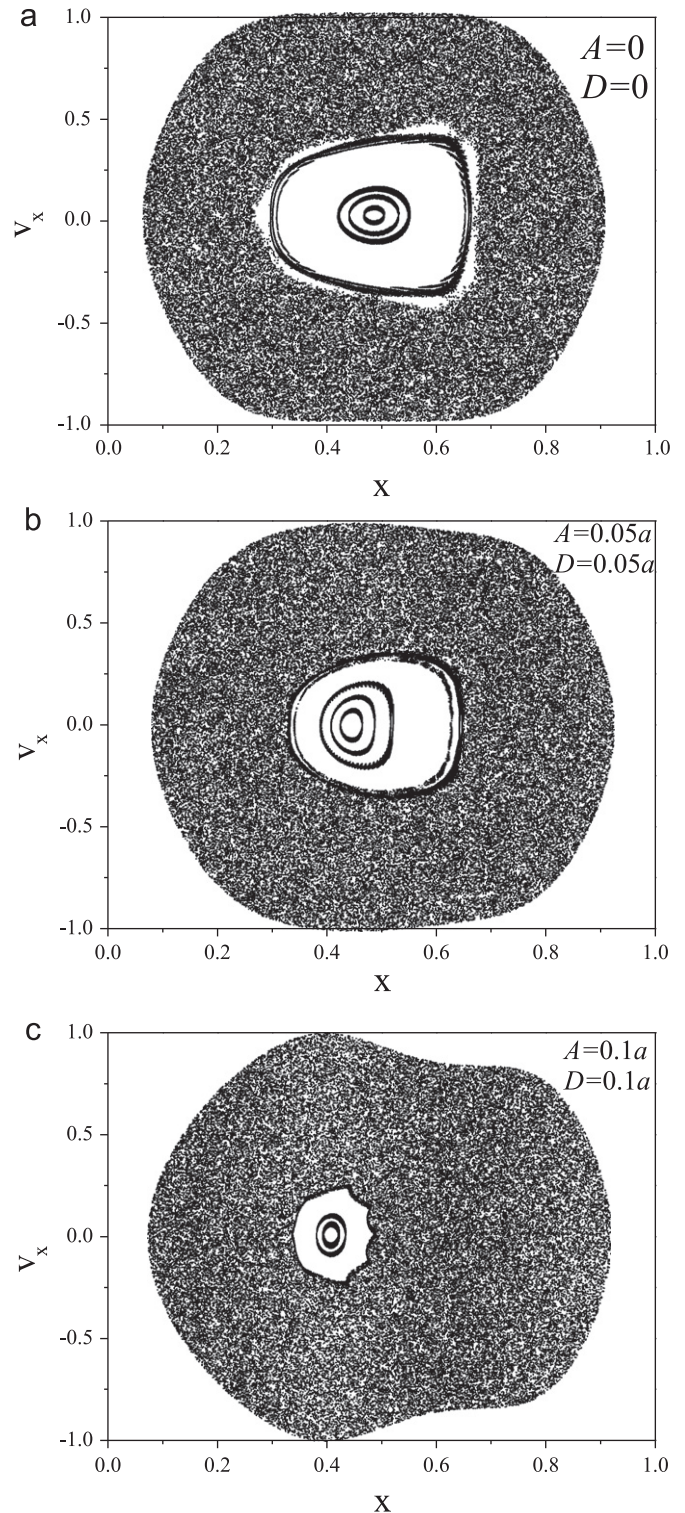


Fig. 7. Three Poincaré surfaces of section at $[y(\text{mod } 1)]=0$ for the 2DEG in perpendicular magnetic field, constrained to the surface $f_1(x,y)$ in a rectangular antidot lattice. (a) $A = D = 0$, (b) $A = D = 0.05a$, (c) $A = D = 0.1a$.

averaged over phase space Γ , the indices i and j stand for the x and y directions, respectively. The presence of additional scattering is included through the electron mean scattering time τ , where the probability of an electron not suffering a collision within the time interval $[0, t]$ is given by $e^{-t/\tau}$. From the numerical computation of the conductivity tensors we are able to determine the longitudinal ρ_{xx} and transverse ρ_{xy} resistivities:

$$\rho_{xx} = \frac{\sigma_{xx}}{\sigma_{xx}\sigma_{yy} + \sigma_{xy}\sigma_{yx}}, \quad (21)$$

$$\rho_{xy} = \frac{\sigma_{xy}}{\sigma_{xx}\sigma_{yy} + \sigma_{xy}\sigma_{yx}}. \quad (22)$$

In order to calculate conductivity, we generate an ensemble of electron trajectories, uniformly distributed inside a square region of one period side.

3. Calculation of longitudinal and transversal resistivities

3.1. Magnetoresistance for the 2DEG constrained to type 1 topography

For f_1 surface with a finite amplitude the non-planar topography introduces an inhomogeneity of the perpendicular component of the magnetic field, the small gradient of the magnetic field gives rise to a force $\vec{F} = -\mu\vec{\nabla}B$ where $\mu = m^*v_{\perp}^2/2B$. v_{\perp} is the component of the velocity of the charged particle perpendicular to the magnetic field vector. This force produces a drift of the guiding center $\vec{v}_{gc} = (m^*v_{\perp}^2)/(2qB^3)\vec{B} \times \vec{\nabla}B$ [19]. When $D=0$ and $A \neq 0$ with $A \ll a$, the topography is formed by periodic hills and valleys along x direction, and the electron trajectories drift along the y direction.

Fig. 2(a) shows the numerical magnetoresistance for the 2DEG constrained to f_1 topography, with $A=0.4a$, $A=0.3a$, $A=0.2a$ maintaining $D=0$, the magnetoresistance ρ_{xx} for this system shows periodic oscillations in B/B_0 and a linear decrease for field values $B/B_0 < 1$. Fig. 2(b) shows the numerical Hall resistance for the same amplitudes, A and D , depicted in part (a), the Hall resistance increase linearly and exhibits small traces of periodic oscillations for field values $B/B_0 > 1$. As D is set different to 0 and the x and y degrees of freedom are coupled, the non-linear

perturbation allows the development of chaos in phase space Γ , consequently, low field oscillations of magnetoresistance are gradually destroyed. Fig. 3 shows two Poincaré maps at $[y(\text{mod } 1)] = 0$ for (a) $A=0.3a$ and $D=0.025a$ and (b) $A=0.3a$ and $D=0.3a$. For $A=0.3a$ and $D=0$ all trajectories are periodic, and the electrons drift in a straight line along y direction. When D is set different from zero chaotic trajectories appear in phase space Γ . When the coupling of the degrees of freedom reaches the same amplitude along the x and y directions the phase space evolves to fully chaotic.

Fig. 4 shows some numerically calculated electron trajectories for the cases: (a) small coupling of the degrees of freedom $A=D=0.05a$, (b) strong coupling $A=D=0.3a$. The curves were calculated for perpendicular magnetic field $\theta = \pi/2$, $\phi = 0$, $B/B_0 = 1$, $U_0 = 0$. For very low coupling of the x and y degrees of freedom the electron trajectories drift along the hills and valleys, as the degree of coupling increases the trajectories in phase space develop a chaotic diffusion.

In order to study the interplay between boundary scattering and geometrical constraints under a steady increase of the degree of disorder the dynamics of a planar 2DEG in a lattice of antidots of period a was calculated in perpendicular magnetic field, the antidot potential was simulated by Eq. (5). The parameters $U_0 = 2.0E_F$, $\beta = 6$, were used in the calculations in order to emulate an experimental situation in which the antidot cross section at the Fermi energy is $d \approx 0.23a$ [20]. After, the topography of the 2DEG was gradually wrinkled following a f_1 surface model, the amplitudes of the corrugations along x and y directions were tuned by means of the A and D parameters. Fig. 5 shows the evolution of ρ_{xx} at low field for $A=D=0$ to $A=D=0.27a$ (curves were dislocated in the vertical direction for better viewing),

When the topography is planar $A=D=0$, the numerical magnetoresistance curve (located at the bottom of figure) displays several commensurability peaks, the main peak is associated with the condition $2R_c = a$ where R_c is the cyclotron radius, other observed peaks are those at the conditions $R_c = 3a$, $R_c = 5a/3$, and $R_c = 0.74a$. When the A and D parameters are gradually increased, and the degree of disorder augments, a pronounced evolution of the ρ_{xx} curves occurs. Three main effects are observed: (a) a shift of the commensurability peaks, (b) a broadening of the commensurability peaks, and

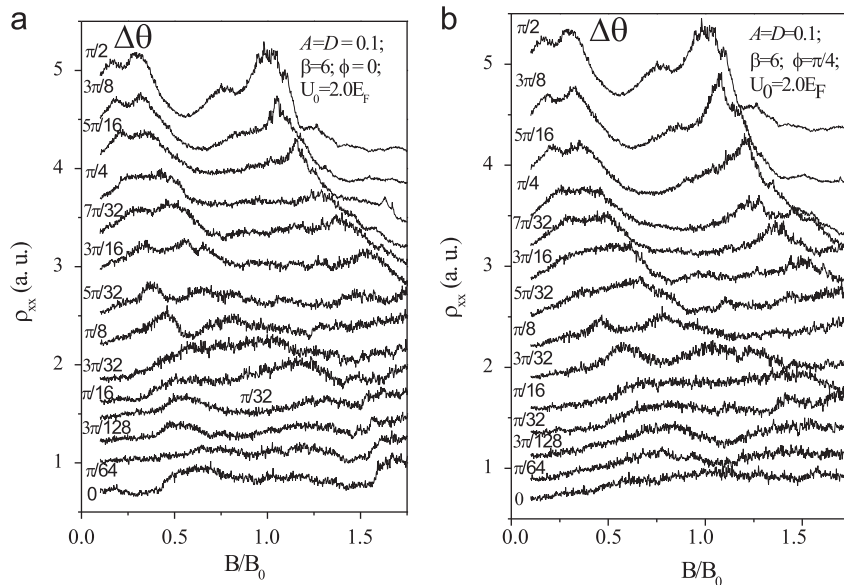


Fig. 8. (a) Numerical ρ_{xx} curves, for a 2DEG constrained to $f_1(x,y)$ topography, in a lattice of antidots and as a function of tilted magnetic field and angle θ , for $A=D=0.1a$, $U_0=2.0E_F$, $\beta=6$ and $\phi=0$. θ varies from $\pi/2$ to 0. (b) The same evolution shown in part (a) this time for $\phi=\pi/4$.

(c) an increase of the longitudinal resistivity for lower values of the magnetic field (negative magnetoresistance). The gradual transformation of the magnetoresistance commensurability peaks to a constant decrease as a function of the degree of disorder is in accord with the experimental situation of samples with a 2DEG constrained to non-planar topographies with a high degree of disorder [14]. For the other side, the shift of the commensurability peaks to higher values of the normalized magnetic field B/B_0 can be attributed to the gradual variation of the cross section of the antidot at the Fermi energy from circular to elliptical. When the 2DEG is planar the shape of the antidot at the Fermi energy is circular, as the topography changes the shape of the antidot evolves from circular to elliptical changing also the commensurability between the cyclotron radius and the period of the lattice. A related effect was observed in the dynamics of a quasi-three-

dimensional electron gas (3DEG) in the presence of cylindrical antidots in tilted magnetic field [21].

Fig. 6 shows a scheme of an antidot unit cell of period a , when the 2DEG topography is planar the cross section of the antidot is circular, as the topography changes by the corrugations the length of the path followed by electrons between neighboring antidots increases even though the distance between the center of them remain the same. The area of the surface contained in a unit cell of period a increases and consequently the area and shape of the antidot cross section also varies.

Following the model for the 2DEG dynamics constrained to f_1 topography in perpendicular magnetic field Poincaré surfaces of section for the case of antidot diameter at the Fermi energy of $d = 0.2a$ were calculated. A Poincaré surface of section at $y = y_0$ is the intersection of the energy surface with the plane $y = y_0$.

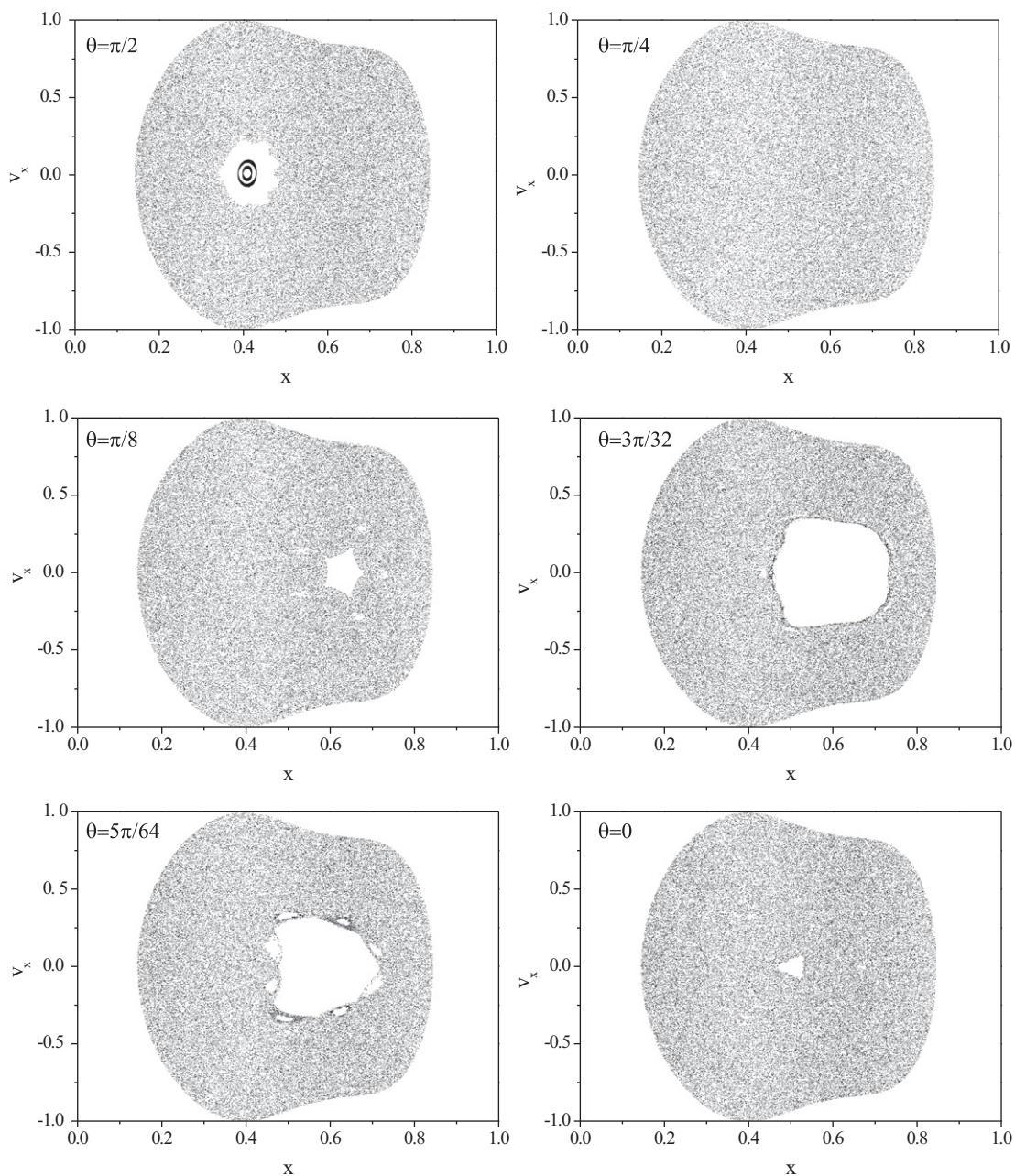


Fig. 9. Six Poincaré surfaces of section at $[y(\text{mod } 1) = 0]$ for the 2DEG constrained to f_1 topography under tilted magnetic field. The parameters used are $A = D = 0.1a$, $U_0 = 2.0E_F$, $\beta = 6$, $\phi = 0$ and $B/B_0 = 1$. From $\theta = \pi/2$ to $\theta = \pi/4$ the phase space turns chaotic, from $\theta = \pi/8$ a stability region is opened reaching its maximum area for $\theta = 3\pi/32$, for lower θ values phase space turns chaotic again.

Fig. 7 shows three Poincaré surfaces of the section at $[y(\bmod 1) = 0]$ for $B/B_0 = 1$ in the smooth potential generated for 20 randomly chosen initial conditions. In the upper part, marked with (a), we have the case of a surface of the section for perpendicular magnetic field ($\theta = \pi/2$, $\phi = 0$) and without corrugation $A = D = 0$. It is possible to observe several islands around $x=0.5$ surrounded by a chaotic sea. The islands correspond to regular motion and, according to the Kolmogorov–Arnold–Moser (KAM) theorem [22] the intersections of invariant tori for cyclotronic orbits with $R_c = a/2$ revolving around the single antidot located at $(x,y) = (0,0)$ are represented. Fig. 7(b), corresponds to a surface of the section, at $[y(\bmod 1) = 0]$, with the same initial conditions as the previous figure, this time, the amplitude of the superficial corrugations was $A = D = 0.05a$. When the geometrical constraint is applied a severe transformation of the electron dynamics occurs, most of the islands of regular motion disappear due to an increase of the degree of chaos of the system and also a deformation of the region of stable motion is observed. Fig. 7(c) shows the Poincaré surface of the section, at $[y(\bmod 1) = 0]$, with the same conditions as the two previous, this time for $A = D = 0.1a$. Most of the regular islands corresponding to periodic motion completely disappeared and a higher increase of the shrinking of the area corresponding to stable motion occurs. The presence of islands surrounded by a self-similar hierarchy of cantori is also observed, these are persistent remnants of KAM tori formed after their destruction as the amplitude of the corrugation increases. Each cantorus forms a Cantor set of points on the surface of section [23]. The shrinking of the stable motion region area can be attributed to the variation of the antidot diameter along the x – y directions, as the commensurability condition $2R_c = a$ is lost due to perturbation of the magneto-focussing effect

some regular orbits will inevitably change to chaotic due to backscattering with neighboring antidots.

The electron dynamics of the 2DEG constrained to the $f_1(x,y)$ topography in the presence of an antidot lattice were also analyzed in tilted magnetic field. Fig. 8(a) shows in the upper part a numerical ρ_{xx} curve calculate with the same parameters as those used in calculations shown in Fig. 5, this time, the amplitudes of corrugations along the x and y directions are fixed to $A = D = 0.1a$ (the amplitudes along the x and y directions are 1% of the antidot lattice period a). Using this curve as a reference the magnetic field vector was gradually tilted from $\theta = \pi/2$ towards the in-plane direction until it reaches the parallel direction, in this case $\theta = 0$ (in both cases $\phi = 0$).

As the magnetic field vector is tilted, in relation to the x – y plane, the perpendicular component of the magnetic field B_{\perp} varies with position. The commensurability peaks are gradually broadened and shifted to higher values of the normalized magnetic field B/B_0 , this occurs between $\theta = \pi/2$ and $\theta = 5\pi/32$. Calculations of the Poincaré surfaces of section in this interval presented in Fig. 9 show that phase space is chaotic, for lower values of θ new commensurability oscillations appear in magneto-resistance curves, this can be attributed to new orbits that become possible due to the additional drift of electron trajectories along the parallel component of the magnetic field along the x direction. Poincaré maps show that a stability region is opened between $\theta = \pi/8$ and $\theta = \pi/32$, for lower values of θ the phase space turns mainly chaotic again.

Magneto-resistance was also calculated with a variation of the direction of tilting of the magnetic field vector. Fig. 8(b) shows the ρ_{xx} evolution from $\theta = \pi/2$ to $\theta = 0$ for $\phi = \pi/4$. In this case, the

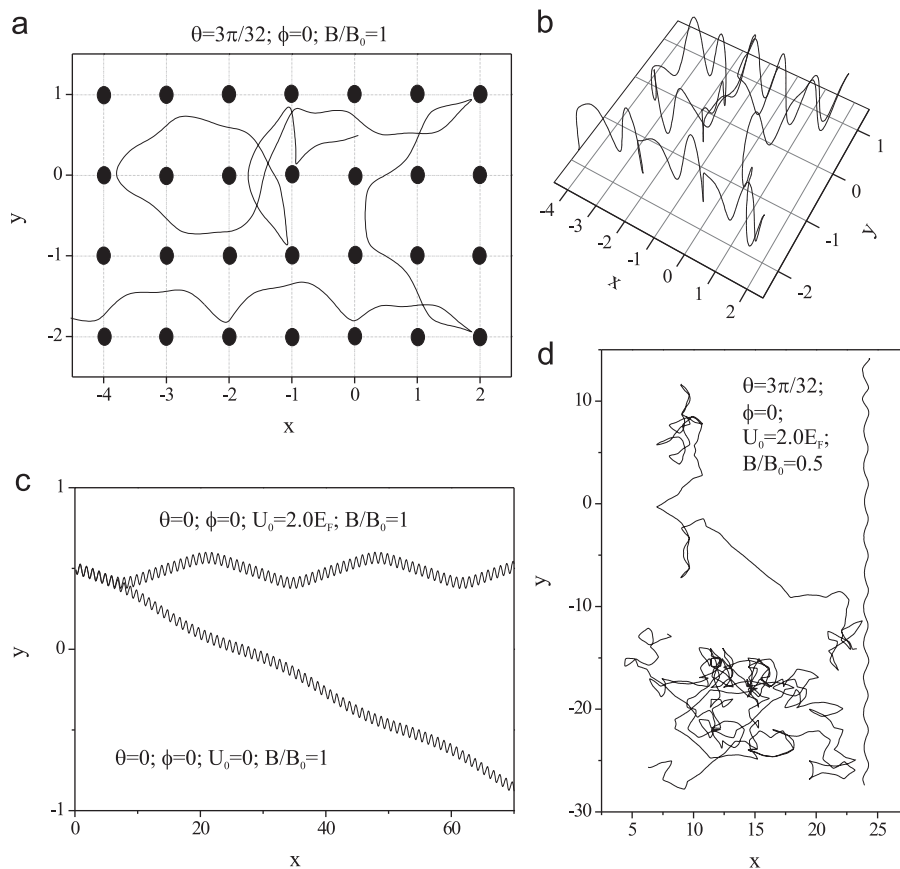


Fig. 10. Some numerical trajectories calculated for f_1 topography in tilted magnetic field, all of them were calculated with $\phi = 0$. (a) Top view for $\theta = 3\pi/32$, $U_0 = 2.0E_F$, $\beta = 6$ and $B/B_0 = 1$. (b) Lateral view of the same trajectory shown in (a). (c) Upper part: top view of a “runaway” trajectory for $\theta = 0$, $U_0 = 2.0E_F$ and $\beta = 6$, lower part: the same trajectory without the antidot lattice. (d) Top view of some chaotic and periodic orbits for $\theta = 3\pi/32$, $U_0 = 2.0E_F$, $\beta = 6$ and $B/B_0 = 0.5$.

magnetic field vector is tilted towards the x – y plane making an angle ϕ of $\pi/4$ with the x -axis. From the comparison of the two evolutions in tilted magnetic field observed in Fig. 8(a) and (b), a dependence of ρ_{xx} with the direction of tilting of the magnetic field vector is observed, this difference begins to be evident for values of the angle θ lower than $3\pi/16$. The commensurability oscillations observed at these angles are not the same and evolve in a different way. The helicoidal trajectories along the x direction are perturbed when the direction of the magnetic field vector is changed as illustrated in Fig. 10.

Fig. 10 shows some numerical trajectories calculated for f_1 topography in tilted magnetic field, all of them were calculated for $\phi = 0$. (a) Top view of an electron trajectory for $\theta = 3\pi/32$, $U_0 = 2.0E_F$, $\beta = 6$ and $B/B_0 = 1$, at this angle, the area of the

stability region reaches its maximum. (b) Lateral view of the same trajectory shown in (a). (c) In the upper part the top view of a three-dimensional “runaway” trajectory for $\theta = 0$, $U_0 = 2.0E_F$ and $\beta = 6$ is shown, in the lower part: the same trajectory, this time, without the antidot lattice. (d) Top view of some chaotic and periodic orbits for $\theta = 3\pi/32$, $U_0 = 2.0E_F$, $\beta = 6$ and $B/B_0 = 0.5$.

3.1.1. Magnetoresistance for the 2DEG constrained to type 2 topography

The magnetoresistance for f_2 topography was also calculated with and without antidot lattices. Fig. 11(a) shows the evolution of the low field ρ_{xx} for different values of the amplitude of the corrugations from $A = 0.03a$ to $A = 1.3a$. The curves were calculated

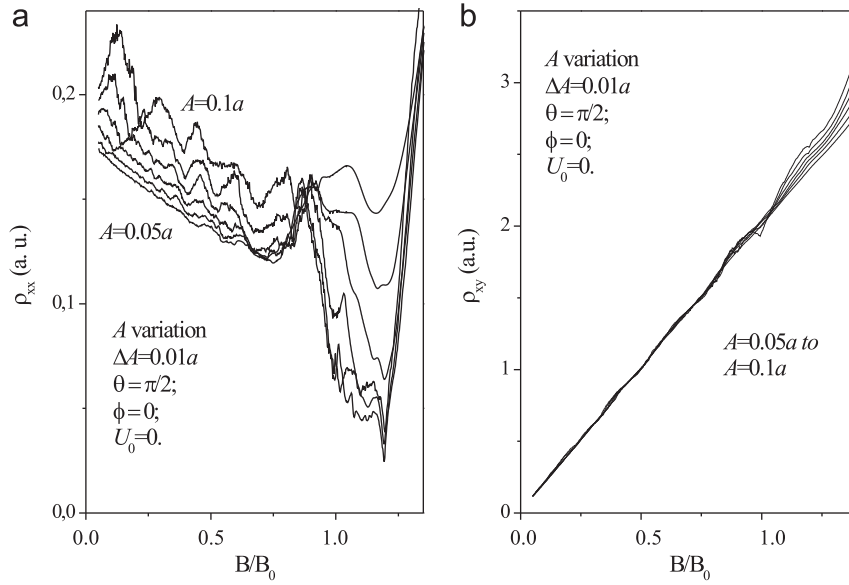


Fig. 11. (a) Magnetoresistance of the 2DEG constrained to $f_2(x,y)$ topography as a function of the amplitude A . The parameters used are $\theta = \pi/2$, $\phi = 0$, and $U_0 = 0$, commensurability oscillations are observed as a function of A and B/B_0 . (b) Evolution of ρ_{xy} as a function of A for the same parameters used in part (a).

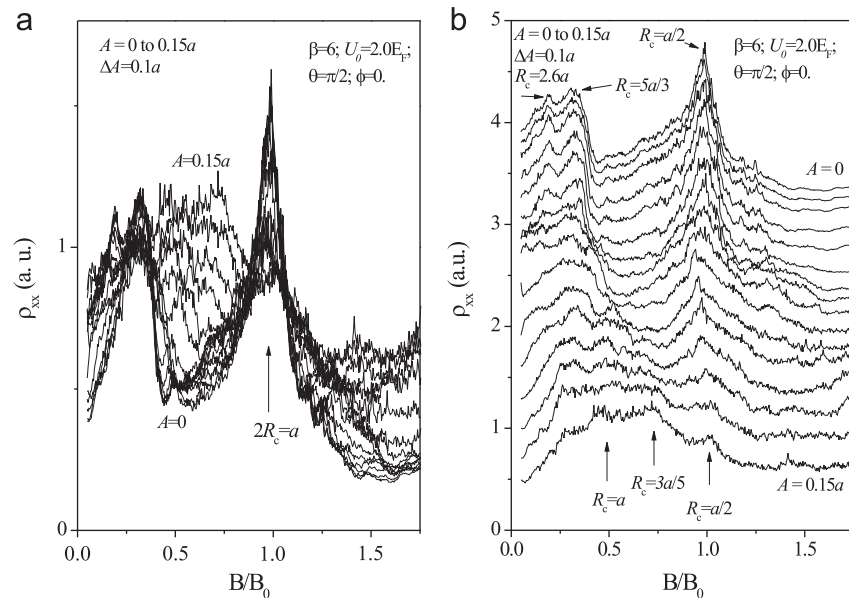


Fig. 12. (a) Magnetoresistance of the 2DEG constrained to f_2 topography in antidot lattice as a function of the amplitude A . The parameters used are $\theta = \pi/2$, $\phi = 0$; $U_0 = 2.0E_F$, and $\beta = 6$. The maximum amplitude A of the corrugations was varied from $A = 0$ to $A = 0.15a$ in steps of $\Delta A = 0.1a$. The low field commensurability oscillations, due to antidot lattice, evolve drastically as a function of A . (b) ρ_{xx} curves shown in (a) this time vertically spaced for better observing the peaks transformation and evolution.

for perpendicular magnetic field $\theta = \pi/2$ and $\phi = 0$, for this topography, the longitudinal resistivities show periodic oscillations whose amplitude depends on the value of the parameters A and B/B_0 , these oscillations are superposed to a background of constant decrease (negative magnetoresistance) for $B/B_0 < 1$. For f_2 there is no preferential drift direction for the charged particles as is the case of f_1 topography when $D=0$. Fig. 11(b) shows the numerical transversal resistivities curves for the same parameters used in part (a). A linear increase of ρ_{xy} for lower values of the normalized magnetic field is observed. Traces of the ρ_{xx} oscillations at higher values of the magnetic field are also observed at the ρ_{xy} curves.

A lattice of antidots was added to the 2DEG constrained to f_2 topography and the behavior of the ρ_{xx} and ρ_{xy} resistivities was calculated and analyzed as a function of the maximum amplitude of the corrugations A . Fig. 12(a) shows this evolution from $A=0$ to $A=0.15a$ in steps of $\Delta A = 0.1a$ for $\theta = \pi/2$, $\phi = 0$, $U_0 = 2.0E_F$, and $\beta = 6$. A completely different evolution of the ρ_{xx} commensurability oscillations from f_1 topography is observed (see Fig. 5). In Fig. 12(b) the curves showed in part (a) were dislocated for a better viewing of the evolution. On top of this figure we have the magnetoresistance for $A=0$, and below the evolution for lower A values. There is no significant shift of the main commensurability peak ($R_c = a/2$), however, the low field ρ_{xx} oscillations located mainly at $R_c = 2.6a$ and $R_c = 5a/3$ are drastically modified, first, with a small increase of A their amplitude also increases then, with a higher increase of the amplitude A new oscillations appear and for $A = 0.15a$ there are two pronounced peaks located at the conditions $R_c = a$ and $R_c = 3a/5$.

The evolution of the magnetoresistance for the 2DEG constrained to f_2 topography shows a different behavior than those presented by f_1 surface. Besides the evolution of the low field commensurability oscillations as a function of A there is another important difference for f_2 topography, the longitudinal resistivity ρ_{xx} does not evolve to negative magnetoresistance with the increment of A , instead a positive behavior was observed for values of A higher than $0.2a$, these results deserve a deeper study and are not presented here. The phase space for the 2DEG constrained to f_2 topography was also analyzed by means of Poincaré surfaces of section. Fig. 13 shows three phase space portraits at $[y(\text{mod } 1)] = 0$ for (a) $A=0$, (b) $A=0.05a$ and (c) $A=0.1a$, in this case $B/B_0 = 1$, $U_0 = 2.0E_F$, $\beta = 6$, $\theta = \pi/2$ and $\phi = 0$. In Fig. 13(a) a Poincaré map for antidot diameter at the Fermi energy of $d = 0.2a$ generated by 30 randomly chosen initial conditions is presented. Several periodic and quasi-periodic orbits surrounded by a stability region and a chaotic sea are observed around $x=0.5$. (b) As the amplitude is set to $A = 0.05a$ ($A = 5\%a$), the regular motion is perturbed and becomes unstable, some periodic and quasi-periodic persist while others turn chaotic. New islands of stability are observed. (c) For $A = 0.1a$ most of the regular islands corresponding to periodic motion completely disappeared and a diminution and deformation of the area corresponding to stable motion occurs, however, the development of chaos in phase space is lower than that in the case of f_1 topography due to a less coupling of the degrees of freedom in λ , Eq. (18).

The numerical longitudinal and transversal resistivities for the 2DEG constrained to the $f_2(x,y)$ topography in the presence of an antidot lattice in tilted magnetic field are presented in Fig. 14. In part (a) the ρ_{xx} evolution from $\theta = \pi/2$ to $\theta = 0$ is presented, the parameters used are: $U_0 = 2.0E_F$, $\beta = 6$, and $\phi = 0$. Three peaks are observed at $\theta = \pi/2$ (topmost curve), the main at $2R_c = a$, one at $R_c = a$ and the other at $R_c = 1.6a$, as the magnetic field vector is tilted a small different behavior to the case of ρ_{xx} evolution for f_1 topography is observed. The commensurability peaks shift to higher values of the magnetic field and broaden as a function of the value of the perpendicular component of the magnetic field in

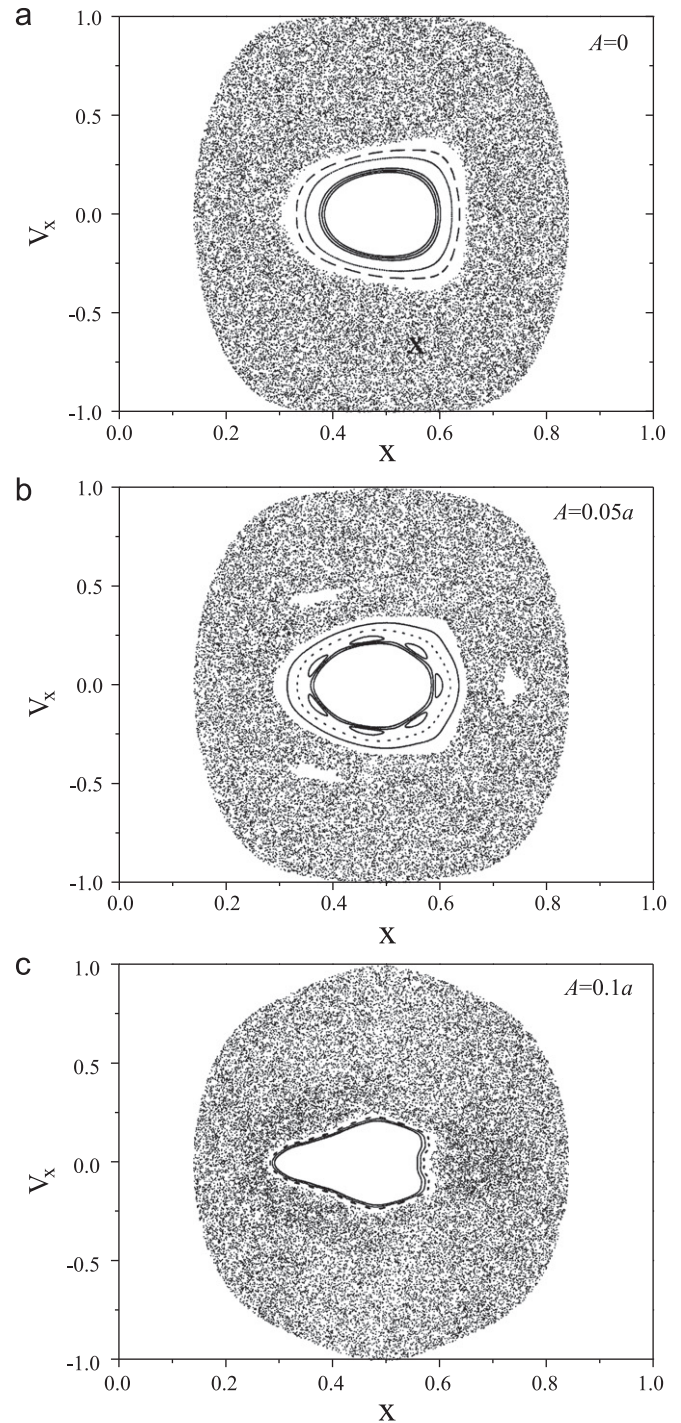


Fig. 13. Poincaré maps as a function of A , for f_2 topography with $B/B_0 = 1$, $U_0 = 2.0E_F$, $\beta = 6$, $\theta = \pi/2$ and $\phi = 0$. In (a) $A = 0$, (b) $A = 0.05a$ and (c) $A = 0.1a$, again, the degree of chaos increases as a function of the corrugation amplitude A .

similar way as a planar 2DEG in tilted magnetic field [20], however, the amplitude of the peaks are greater for f_2 topography than for f_1 in almost parallel magnetic field. In part (b) the evolution of the ρ_{xy} curves, for the same parameters used in part (a), is also presented.

4. Summary

We have numerically studied the classical dynamics of a two-dimensional electron gas, under uniform magnetic field, in

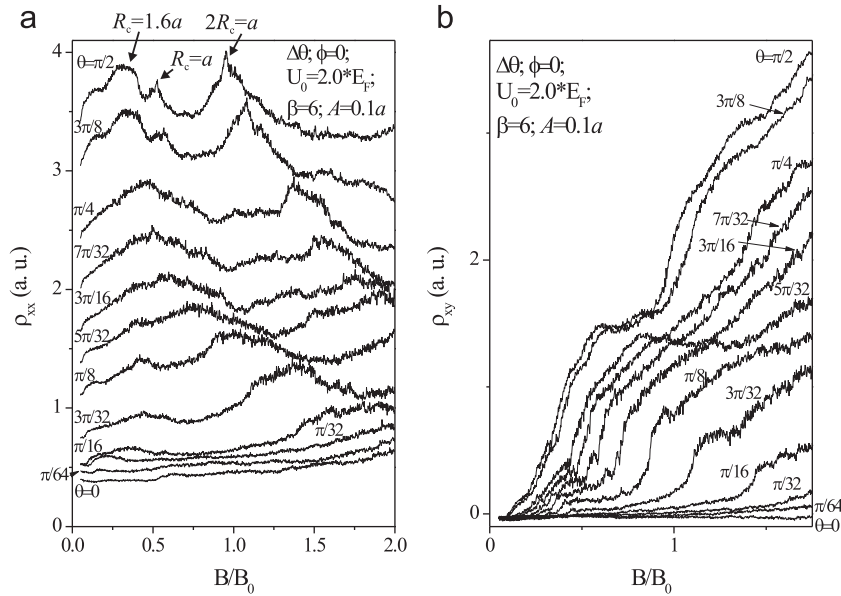


Fig. 14. (a) Numerical ρ_{xx} curves, for a 2DEG constrained to f_2 topography, in a lattice of antidots and as a function of tilted magnetic field, for $B/B_0 = 1$, $U_0 = 2.0E_F$, $\beta = 6$, $\theta = \pi/2$ and $\phi = 0$. (b) Numerical ρ_{xy} curves for data in part (a).

antidot lattice, when subjected to periodic geometrical constraints that change the topography of the 2DEG from planar to non-planar. The results show that geometrical constraints introduce additional drift, more disorder, coupling of the guiding center in the x and y directions and consequently additional chaos on phase space. The low field magnetoresistance commensurability oscillations due to antidot lattice are strongly affected by the introduction of geometrical constraints, their evolution show that depending on the amount of coupling of the degrees of freedom introduced by the topographies through the Lagrange multiplier λ , the ρ_{xx} curves can evolve to a destruction of the commensurability peaks and a transformation to a completely negative behavior, as shown by the experiments in the literature. Also, the longitudinal resistivity for the 2DEG, constrained to non-planar topographies in antidot lattice and tilted magnetic field shows dependence with the direction of the parallel component of the magnetic field.

Acknowledgments

This work was partially supported by CNPQ (National Counsel of Technological and Scientific Development) Brazilian Funding Agency and used computational facilities of CENAPAD-SP (Centro Nacional de Processamento de Alto Desempenho, UNICAMP/FINEP-MCT Project).

References

[1] J.E. Müller, *Physical Review Letters* 68 (1992) 385.
 [2] T. Sugiyama, N. Nagaosa, *Physical Review Letters* 70 (1993) 1980.
 [3] A.G. Aronov, E. Altshuler, A.D. Mirlin, P. Wölfle, *Europhysics Letters* 29 (1995) 239.

[4] A.G. Aronov, E. Altshuler, A.D. Mirlin, P. Wölfle, *Physical Review B* 52 (1995) 4708.
 [5] F.B. Mancoff, L.J. Zielinski, C.M. Marcus, K. Campman, A.C. Gossard, *Physical Review B* 53 (1996) R7599.
 [6] A.D. Mirlin, J. Wilke, F. Evers, D.G. Polyakov, P. Wölfle, *Physical Review Letters* 83 (1999) 2801.
 [7] P.D. Ye, D. Weiss, R.R. Herdhardt, M. Seeger, K. von Klitzing, K. Eberl, H. Nickel, *Physical Review Letters* 74 (1995) 3013.
 [8] A. Nogaret, S.J. Bending, M. Henini, *Physical Review Letters* 84 (2000) 2231.
 [9] M.L. Leadbeater, C.L. Foden, J.H. Burroughes, M. Pepper, T.M. Burke, L.L. Wang, M.P. Grimshaw, D.A. Ritchie, *Physical Review B* 52 (1995) R8629.
 [10] H.A. Carmona, A.K. Geim, A. Nogaret, P.C. Main, T.J. Foster, M. Henini, S.P. Beaumont, M.G. Blamire, *Physical Review Letters* 74 (1995) 3009.
 [11] G.M. Gusev, U. Gennser, X. Kleber, D.K. Maude, J.C. Portal, D.I. Lubyshv, P. Basmaji, M de P.A. Silva, J.C. Rossi, Yu.V. Nastaushev, *Superlattices and Microstructures* 18 (1995) 67.
 [12] G.M. Gusev, J.R. Leite, A.A. Bykov, N.T. Moshegov, V.M. Kudryashev, A.I. Toropov, Yu.V. Nastaushev, *Physical Review B* 59 (1999) 5711.
 [13] A.A. Bykov, G.M. Gusev, J.R. Leite, A.K. Bakarov, N.T. Moshegov, M. Cassé, D.K. Maude, J.C. Portal, *Physical Review B* 61 (2000) 5505.
 [14] N.M. Sotomayor, G.M. Gusev, J.R. Leite, A.A. Bykov, A.K. Kalagin, V.M. Kudryashev, A.I. Toropov, *Physical Review B* 70 (2004) 235326.
 [15] A.V. Bobylev, F.A. Maaø, A. Hansen, E.H. Hauge, *Journal of Statistical Physics* 87 (1997) 1205.
 [16] N.M. Sotomayor, J.F. da Rocha Neto, G.M. Gusev, *Brazilian Journal of Physics* 36-2A (2006) 340.
 [17] P.A.M. Dirac, *Lectures on Quantum Mechanics*, Belfer Graduate School of Science, Yeshiva University, New York, 1946.
 [18] R. Kubo, M. Toda, N. Hashitsime, *Statistical Physics II*, Springer-Verlag, Berlin, 1985.
 [19] H. Alfvén, *Cosmical Electrodynamics*, Clarendon Press, Oxford, England, 1950.
 [20] N.M. Sotomayor Choque, G.M. Gusev, J.R. Leite, A.A. Bykov, L.V. Litvin, N.T. Moshegov, A.I. Toropov, D.K. Maude, J.C. Portal, *Physical Review B* 66 (2002) 035324.
 [21] N.M. Sotomayor, G.M. Gusev, J.R. Leite, A.A. Bykov, L.V. Litvin, N.T. Moshegov, A.I. Toropov, O.Estibals, J.C. Portal, *Physical Review B* 67 (2003) 113308.
 [22] M.V. Berry, in: S. Jorna (Ed.), *Topics in Nonlinear Dynamics*, American Institute of Physics, New York, 1978 (AIP Conference Proceedings, vol. 46).
 [23] C. Efthymiopoulos, G. Contopoulos, N. Voglis, *Celestial Mechanics and Dynamical Astronomy* 73 (1999) 221.